ICARUS **131,** 107–122 (1998)
ARTICLE NO. IS975856

Measurement and Analysis of Lunar Basin Depths from Clementine Altimetry

Kevin K. Williams[1]

Department of Earth and Planetary Sciences, Johns Hopkins University, Baltimore, Maryland 21218
E-mail: kkw@asu.edu

and

Maria T. Zuber

Department of Earth, Atmospheric, and Planetary Sciences, Massachusetts Institute of Technology, Cambridge, Massachusetts 02139-4307; and Laboratory for Terrestrial Physics, NASA/Goddard Space Flight Center, Greenbelt, Maryland

Received April 3, 1997; revised August 22, 1997

Altimetric profiles from the Clementine LIDAR are used to calculate the depths of 29 large craters and basins on the Moon. Plotting the depths of the best preserved structures together with values for simple and complex craters measured in pre-Clementine studies reveals an inflection in the depth/diameter (*d*/*D*) curve in addition to the one revealed by pre-Clementine data. This inflection occurs in the diameter range that corresponds to the morphologic transition from complex crater to basin. The best empirical power law fit for basin depths is $\log_{10}(d) = 0.41 \times [\log_{10}(D)]^{0.57}$. This relationship is characterized by a lower slope than that for complex craters, demonstrating that this morphologic transition corresponds to a further decrease in the depth of an impact structure relative to its diameter with increasing size. Qualitative consideration of possible causes for the second inflection leads to the conclusion that it is most likely a consequence of a short-term modification mechanism that influences fundamental crater morphology, such as the increasing influence of gravity with diameter. Thicknesses of maria in the major basins are calculated by assuming that their unfilled depths would follow the *d*/*D* relation. Results are compared with previous estimates and yield thicknesses that are generally greater than those determined by studies of flooded craters and less than those obtained from analysis of gravity. © 1998 Academic Press

Key Words: **moon; moon surface; cratering; impact processes; collisional physics.**

INTRODUCTION

Major impacts added a significant amount of energy to the Moon during the period of heavy bombardment in the Moon's early evolution (Safronov 1972, Kaula 1979). The geometries and subsurface structures of large impact basins preserve a record of the mechanics of impact, the nature of basin modification, and the thermal and physical properties of the early Moon. Until recently, the geometries of major basins could not be studied in detail in a collective sense because uniform, high quality topographic coverage did not exist. Recently, the Clementine mission (Nozette *et al.* 1994) provided near-global topography (Zuber *et al.* 1994, Smith *et al.* 1997) which is analyzed here to determine the depths of major lunar basins. From the measurements, we derive a basin depth/diameter (*d*/*D*) relationship which is used to address first order implications for the processes that control basin morphology and to place constraints on the thicknesses of the maria in major basins.

CRATER DEPTH: MORPHOLOGY AND CONTROLLING MECHANISMS

Prior to the Clementine mission, the principal topographic data set for studies of lunar impact structures was compiled by NASA and the U.S. Defense Mapping Agency in the form of 1 : 250,000 lunar topographic orthophotomaps (LTOs). These contour maps were based on metric camera images from Apollos 15–17 and have a precision of approximately ±25–70 m, depending on the map.

In evaluating fresh lunar craters, Pike (1974) used the LTOs as well as other relative topographic data to measure dimensions of simple and complex craters and showed that a power law relation exists between the rim-to-floor depth of a crater and its rim-to-rim diameter. The data revealed the existence of an inflection in the logarithmic plot of depth versus diameter over a diameter range corresponding to the transition from simple to complex crater mor-

[1] Present address: Department of Geology, Arizona State University, Tempe, Arizona 85287-1404.

0019-1035/98 $25.00

phology. This transition, which occurs at a diameter of approximately 15 km on the Moon, is characterized by slumping of the crater walls that results in rim terraces and the formation of a central peak in larger craters. These structural modifications produce a decrease in the depth of a crater relative to its diameter as compared to simple, bowl-shaped craters (Pike 1974). It is generally agreed that rim slumping and floor uplift are non-static processes initiated when the walls of the crater become gravitationally unstable and collapse downward, inward, and then upward in the center producing crater topography which is gravitationally stable (Quaide *et al.* 1965, Dence 1971, Howard 1974, Gault *et al.* 1975, Melosh 1977, 1980, 1982, Malin and Dzurisin 1978, Settle and Head 1979). The slumping of the rim increases the rim crest diameter of the crater (by as much as 30%) while decreasing its depth, reducing the ratio of depth to diameter (Settle and Head 1979) and resulting in the change in slope of the depth/diameter curve at the simple to complex crater transition.

Because craters undergo further transitions in morphology with increasing diameter (i.e., complex to peak-ring to multiring) (Head 1977, Malin and Dzurisin 1978, Settle and Head 1979, Hale and Grieve 1982, Wilhelms 1987, Melosh 1989, Spudis 1993), other adjustments in the depth/diameter curve reflecting those transitions might be expected. It has been proposed that the transition from complex crater to basin begins over a diameter range of 51–80 km where concentric rings of floor roughening first appear around central peaks (Hale and Grieve 1982). While it has been suggested that floor roughening is the early form of peak rings (Hartmann and Wood 1971, Wood and Head 1976, Hale and Grieve 1982, M. J. Cintala, pers. commun. 1996), the distribution of points in this region of the depth/diameter curve for the freshest complex craters does not show conclusive evidence for a change in a crater's depth relative to its diameter (Fig. 1 in Pike 1974).

If the effect on morphology of continued gravitational collapse with increasing diameter is similar to that seen for the simple to complex transition, then the anticipated result of the transition to basin morphology would be a further decrease in the slope of the depth/diameter curve (Melosh 1989). In order to detect such a signature, if it exists, the depth/diameter curve should extend to diameters where basins have fully formed ($D > 150$ km) (Stuart-Alexander and Howard 1970, Hartmann and Wood 1971). However, pre-Clementine topographic data were most often characterized by significant long wavelength biases and did not cover many basins in that size range. Therefore, the limited topographic coverage prevented depth measurements of large lunar craters and basins and the determination of a depth/diameter relationship for them. In contrast, the most recent topographic model of the Moon from the Clementine LIDAR measurements (Zuber *et al.* 1994, Smith *et al.* 1997) includes at least partial coverage of nearly all large lunar basins. We are thus motivated to use this new data set to investigate the depth/diameter relationship for large lunar impact structures.

DATA

Near-globally distributed measurements of geodetically referenced lunar topography were provided by the LIDAR instrument included in the Clementine spacecraft payload (Nozette *et al.* 1994). During the 2-month lunar mapping mission, the Clementine LIDAR determined the range from the spacecraft to the lunar surface by measuring the round trip time of flight of infrared (1.064 μm) pulses from a Nd : YAG laser. The LIDAR range observations have a shot-to-shot precision of 39.972 m dictated by a 14-bit counter in the receiver electronics that binned four cycles of the system oscillator (Smith *et al.* 1997). Lunar radii derived from the range observations after corrections for spacecraft position and orientation have an absolute accuracy with respect to the Moon's center of mass of approximately 100 m (Lemoine *et al.* 1995). This accuracy is controlled to first order by knowledge of the Clementine spacecraft orbit. Data points are distributed in orbital tracks separated by approximately 2.5° (~76 km at the equator) in longitude, with valid ranges obtained within the approximate latitude range from 81°N to 79°S.

The nominal 0.6-Hz pulse repetition rate of the LIDAR, combined with the 2.7 km s^{-1} spacecraft velocity near the periselene altitude of ~500 km, correspond to a shot spacing along the Clementine ground track of approximately 4 km assuming a 100% pulse detection rate. However, the Clementine LIDAR was a military ranging device that was not designed to track continuously non-ideal or variable surfaces. The system worked by leading edge detection of accumulated photons from backscattered laser pulses, but unlike other spacebased laser ranging devices (Zuber *et al.* 1992, Cole *et al.* 1998, Garvin *et al.* 1998), the system electronics did not have the capability to autonomously adjust the detection threshold to accommodate continual changes in orbital geometry, surface albedo, and instrument gain (cf. Zuber *et al.* 1994). The lack of optimization of the receiver function during the ranging sequence resulted in missed detections and false returns triggered by system noise or spurious scattered photons at the laser wavelength; the instrument triggered on 19% of the returned pulses (Zuber *et al.* 1994) and 36% of those returns were attributed to noise and discarded. Noise hits were excluded using a Kalman filter, based on the fractal characteristics of lunar topography, that was applied forward and backward along track (Smith *et al.* 1997). Valid returns from the smooth, dark maria reached as high as 90% in some regions, but the percentage of successful returns was typically much lower on the rough, bright highland terrains. Concerns about the ability of the LIDAR to detect systematically

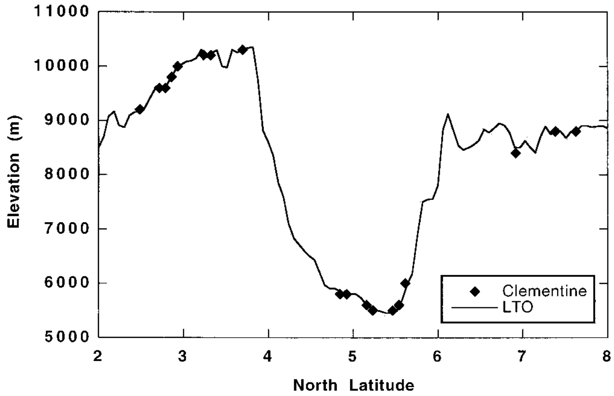

FIG. 1. Clementine LIDAR returns plotted against a digitized profile over King (5°N, 121°E), a very fresh crater with $D = 77$ km. The digitized topography is taken from lunar topographic orthophotomaps (LTO65C1 and LTO65C4) across a profile matching the orbital track from which the LIDAR points were taken. Note that the LIDAR track did not cross over the central peak of King. Details of the Clementine LIDAR profile data are given in Smith *et al.* (1997).

crater rims, which are the roughest of all lunar landforms at the length scale of the along-track shot spacing, have previously been noted (Zuber *et al.* 1994). However, our analysis, which considers the limitations of the data discussed above, indicates that the number of orbital passes over large structures did, in fact, result in an adequate number of reliable rim height measurements to make an analysis of basin depth feasible.

The spatial resolution of the global topographic grid was limited by the spacing of orbital tracks, so we measured the depths of craters and basins using the LIDAR profile data, which were typically characterized by higher resolution. In order to verify that the laser ranging device adequately detected crater rims, we compared Clementine LIDAR profiles to profiles taken from the LTOs for 12 craters with diameters from 52 to 275 km that were also measured by Pike (1974, 1976). For each orbital pass over a crater, the longitude, latitude, and elevation of the filtered LIDAR returns were compiled, and the coordinates were used to read elevations from the LTOs that could be compared to the Clementine elevations. For the smaller craters, the LIDAR tracks crossed either near the rim or just outside the crater. While these topographic profiles did not yield depths, they did give comparisons of LIDAR and LTO profiles for rough terrains. The larger craters and basins had at least one good LIDAR track which detected the rim and floor, resulting in a comparison of depth using the two data sets. Figure 1 illustrates a typical comparison of Clementine points to a profile taken from the LTOs. The comparisons show that Clementine LIDAR profiles agree to within ±100 m of the LTO profiles and verify that the Clementine topography, when analyzed judiciously, can provide measurements of the first order shapes of large craters and basins from which depths can be extracted at quantifiable levels of statistical confidence.

MEASUREMENT OF CRATER AND BASIN DEPTHS

In order to obtain the most accurate relationship between crater depths and diameters, the largest possible number of data points is desired. The Clementine LIDAR sampled many lunar craters, but in order to be eligible for measurement, each candidate crater had to have at least one orbital pass over the central area of the crater in which both the rim and the floor were detected. After examining nearly 100 large craters and basins, only 29 were found to meet this criterion. For each crater, the positions of the LIDAR returns were plotted over an airbrushed map of the region to compare the positions of the LIDAR detections with the basin geometry. An example comparison is provided in Fig. 2. The portions of the individual orbital tracks over the crater were extracted from the global data set and plotted to measure the depth from rim crest to crater floor. To arrive at the most accurate depth estimates, the position of each pass over the crater or basin was compared to Apollo or Earth-based images of the area to detect any outside influence on the depth such as topographic highs or lows due to rims, floors, or ejecta of other craters. If measurement of the rim or floor elevation was obscured by another crater, the affected portion of the profile was not used in determining the depth.

Croft (1981) showed that impact structures undergo a continuous morphologic transition from complex crater to peak-ring basin to multiring basin and concluded that the main outer rims in basins are structurally equivalent to the main rims in complex craters. We therefore used the main outer rims as defined by Wilhelms (1987) to define diameters of the basins. For each of the 29 craters and basins measured, the unobscured elevations of the rim were taken from the plotted orbital tracks to determine the average rim height. The mean floor elevation was calculated using profiles covering the area near the center of the crater, and, following Pike (1974), the depth was calculated by measuring the difference between the mean rim height and the floor elevation.

Because our method of measuring rim heights utilizes a combination of published diameters and photo-interpretation to determine which returns in an orbit are delineating the rim, there is an error associated with the rim height estimation that translates into an error in the calculated depth. This error varies between craters depending on the number of orbital tracks used and how well the LIDAR detected the rim. The measurement of floor elevations has an error associated with it as well, but the error is generally less than 100 m because the flatness of the crater floors results in a large number of LIDAR returns. The floor elevation error was always less than the rim elevation error

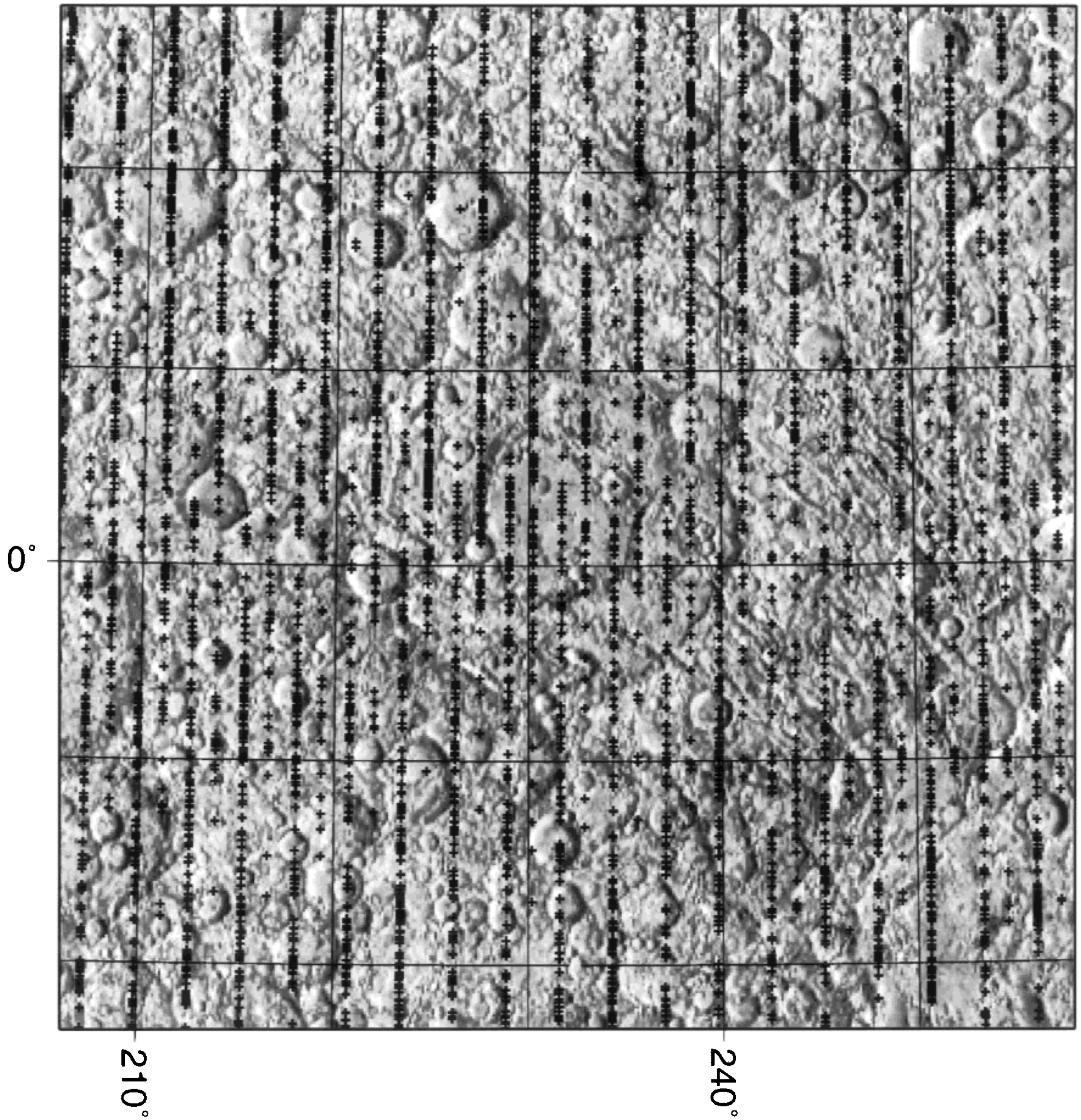

FIG. 2. Locations of filtered LIDAR returns (denoted by +'s) superimposed over an airbrushed map of the region surrounding the Hertzsprung basin (1.5°N, 231.5°E, $D = 570$ km). The LIDAR return positions illustrate that, with many orbital passes over a basin, there were often an adequate number of valid rim returns to measure basin depth.

because of the advantage gained from using the inverse of the square root of the number of observations to reduce error. The error in the depth estimate was taken to be the root sum square of the weighted measurement error and the ~40-m shot-to-shot error of the LIDAR (Smith *et al.* 1997). Table I lists the diameters, depths, associated errors, and ages of the 29 craters and basins measured using Clementine LIDAR data. Diameters and relative ages were taken from Wilhelms (1987). We also analyzed whether the basin diameter measurements from Wilhelms (1987) could be refined from the Clementine altimetric profiles or the global grid but concluded that, given the irregular sampling of the rims on a global and crater-by-crater basis, previous photogeological estimates could not be demonstrably improved.

DEPTH/DIAMETER RELATIONSHIP

The relationship between depth and diameter provides information on post-impact basin mechanics. When considered in the context of basin morphology, such measurements provide a quantitative basis for understanding the

TABLE I
Large Complex Craters and Basins Measured with Clementine Topographic Profiles

Basin	Diameter (km)[a]	Depth (km)	Error (km)	Relative age[a]	Notes
King	77	4.50	0.30	Copernican	
Tycho	85	4.70	0.11	Copernican	
Aristoteles	87	4.00	0.20	Erasthian	
Sklodowska	128	4.45	0.20	Upper Imbrium	Transitional
Langrenus	132	4.55	0.26	Erasthian	Transitional
Compton	162	3.85	0.16	Lower-Imbrium	Upwarped floor
Hausen	167	5.30	0.20	Erasthian	Transitional
Hilbert	178	4.60	0.22	Nectarian	Transitional
Tsiolkovsky	180	4.85	0.11	Upper-Imbrium	Mare
Humboldt	207	3.69	0.38	Upper-Imbrium	Upwarped floor
Landau	221	4.15	0.18	Pre-Nectarian	
Campbell	225	4.40	0.16	Pre-Nectarian	Mare
Clavius	225	4.67	0.32	Nectarian	
Milne	262	3.25	0.15	Pre-Nectarian	Heavily cratered
Bailly	300	4.86	0.44	Nectarian	
Schrödinger	320	4.80	0.12	Lower-Imbrium	
Planck	325	4.00	0.20	Pre-Nectarian	Heavily cratered
Mendeleev	330	4.98	0.16	Nectarian	
Birkhoff	330	4.76	0.19	Pre-Nectarian	
Lorentz	360	4.45	0.24	Pre-Nectarian	Heavily cratered
Korolev	440	5.43	0.65	Nectarian	
Moscoviensce	445	5.25	0.50	Nectarian	Mare
Coulomb-Sarton	530	4.50	0.20	Pre-Nectarian	Heavily cratered
Ingenii	560	4.50	0.20	Pre-Nectarian	Mare
Hertzsprung	570	5.31	0.77	Nectarian	
Humboldtianum	600	4.20	0.20	Nectarian	Mare
Freundlich-Sharonov	600	6.00	1.12	Pre-Nectarian	Heavily cratered
Mendel-Rydberg	630	5.24	0.87	Nectarian	
South Pole-Aitken	2500	8.53	0.53	Pre-Nectarian	Largest Basin

[a] From Wilhelms (1987).

processes that contribute to shallowing of depth relative to diameter with increasing basin size. In addition, by assuming that mare basins would obey the d/D relation if they did not contain mare fill, the relation can be used to estimate the thicknesses of maria in large basins using an approach which differs from previous studies that utilized partially flooded impact craters and gravity data. Accurate measurements of basin depths in combination with information on the compensation states and crustal structure of the major basins can be used in combination with global-scale geochemical (e.g., Lucey *et al.* 1995) and other remote sensing information to understand the spatial and temporal variation of the lunar thermal state.

The values from Table I are plotted along logarithmic axes in Fig. 3 together with previous data for simple and complex craters (Pike 1976). Among the 29 structures measured using Clementine topographic data, 26 have diameters greater than 100 km and traverse the change in morphology from complex crater to multiring basin. Four of those impact structures are complex craters which exhibit some floor roughening (Wilhelms 1987, M. J. Cintala, pers. commun. 1996).

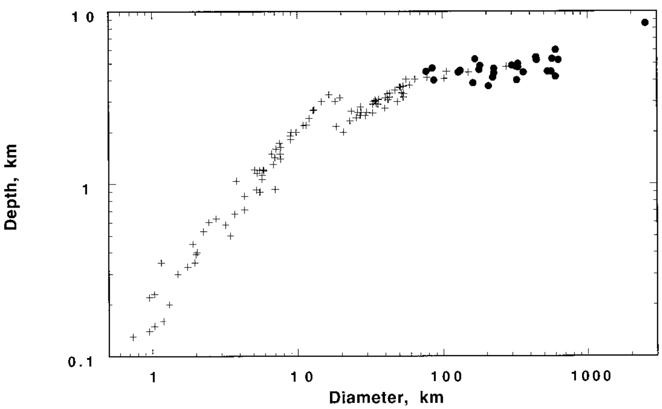

FIG. 3. Depth versus diameter plot for simple craters, complex craters, and basins on the Moon. Data taken from LTOs (Pike 1976) are plotted with +'s while depths measured using Clementine data are denoted by solid circles. A change in slope of the data over a diameter range of 100–200 km (the range over which peak-rings appear) corresponds to the transition from complex crater to basin morphology.

Although the traditional definition of a lunar basin is an impact structure with at least two well-defined rings (Wilhelms 1987, Melosh 1989, Spudis 1993), a second ring is distinct only in craters with diameters greater than 300 km. Craters with diameters between 100 and 300 km exhibit a gradual change from complex crater to multiring basin, some possessing characteristics of both morphologies (Spudis 1993). The transition from complex morphology in fact begins with floor roughening, which is believed to represent the early stages of peak-ring formation (M. J. Cintala, pers. commun. 1996), and becomes more prominent with increasing diameter (Croft 1981, Hale and Grieve 1982). The impact structures spanning the transition from complex crater to basin have been referred to as protobasins by Pike (1983) and form a continuous trend in which more rings appear as the diameter increases (Croft 1981).

Given the increase in complexity of crater morphologies at diameters of approximately 150 and 300 km (Wilhelms 1987), we examined whether either (or both) transition(s) would be evident in the depth/diameter curve. Figure 3 shows that the complex to protobasin transition is obvious as an inflection in the d/D curve with some craters in the diameter range of 100–200 km being transitional. However, while further morphologic evolution from protobasin to multiring basin is observed in images, there is no obvious signature of this transition in the d/D curve. In classifying impact structures, those which are more evolved than complex craters and which traverse the transition to multiring basin have therefore been grouped together as basins.

It should be noted that the break in slope identified here is not an artifact of a change at large (100-km) diameter from LTO-derived depths to Clementine-derived depths. Note that Fig. 3 contains some fresh complex crater depths determined from Clementine data which follow the slope derived from the LTOs. In addition, the (albeit limited) LTO-derived basin depths (Pike 1974, 1976) follow the trend for those structures that have been identified in the Clementine data. Some craters in the transition zone begin to show a departure from the d/D curve for complex craters which is most likely due to the decrease in crater depth associated with concentric floor roughening (Hale and Grieve 1982). Hausen—the largest, fresh complex crater (D = 167 km) (Wilhelms 1987)—falls in the transition zone, exhibiting some floor roughening. However, the depth of Hausen falls only slightly below the d/D relation for complex craters (Pike 1974). If the break in slope were due to the change in data sets, it would be expected that the depth of Hausen measured from Clementine LIDAR profiles would fall on the curve for basin depths. Because depths from LTO and LIDAR data sources do not fall exclusively along data set-specific lines but instead intermix in a region of morphologic transition, the second break in slope cannot be the result of a change in data sets. Instead, the inflection of the d/D curve at the transition from complex crater to basin morphology is likely due to basin formation processes which begin to show surface signatures at diameters of approximately 100 km. These processes may be due to an increase in the effects of gravity for basins of increasing diameter (Melosh 1989) and could perhaps be influenced by interaction of the transient cavity with the lunar Moho (Williams and Greeley 1997).

As for simple and complex craters (Pike 1974), we seek an empirical depth/diameter relationship for basins. In deciding which depths to include in the determination, it is essential to take into account the degree of basin preservation. To arrive at his widely used empirical relationship, Pike (1974, 1976) included the freshest simple and complex craters, noting that he rejected some craters that were "highly subdued." Similarly, there are a number of basins that, for various reasons, have obviously been shallowed. Examination of images revealed that five of the basins measured contain mare fill and one has an upwarped floor (Table I). Both mare filling and floor doming decrease the depths of craters and basins, so these six structures were excluded from the determination of the d/D relationship. Also excluded were basins of pre-Nectarian age, because the early Moon may have had an enhanced thermal structure (Solomon 1986), possibly resulting in a low enough lithospheric viscosity so that these basins are the most likely to have undergone topographic relaxation over geologic time (Solomon *et al.* 1982). Also, most of the pre-Nectartian basins measured have been degraded by subsequent impacts. In addition, because its immense dimensions set if off in a class of its own, the South Pole–Aitken basin was not used in defining the relationship. The remaining seven basins are preserved well enough to be used in finding a relationship explaining the change in basin depth with increasing diameter. While the number of remaining basins constitutes a small statistical sample, we are compelled to limit the analysis to structures that are adequately sampled and well preserved.

Figure 4 shows profiles of the basins used to define the depth/diameter relationship. Each of the seven basins has several orbital passes that were used to measure the depth. The latitudes of LIDAR data in the orbits over each basin were adjusted to appear as though the compiled data were measured over the center of the basin, and the orbit numbers from which the data were taken are listed. The three basins with the largest diameters show a statistically significant difference between their north and south rim heights. Following the precedent established by Pike (1974), the depths for those basins were taken to be the average of the depths taken from both the north and south rim. The error associated with the depth takes into account the difference in rim heights; however, we note that a basin depth/diameter relationship which uses the maximum depths for those three basins would also have a slope less than that for complex craters.

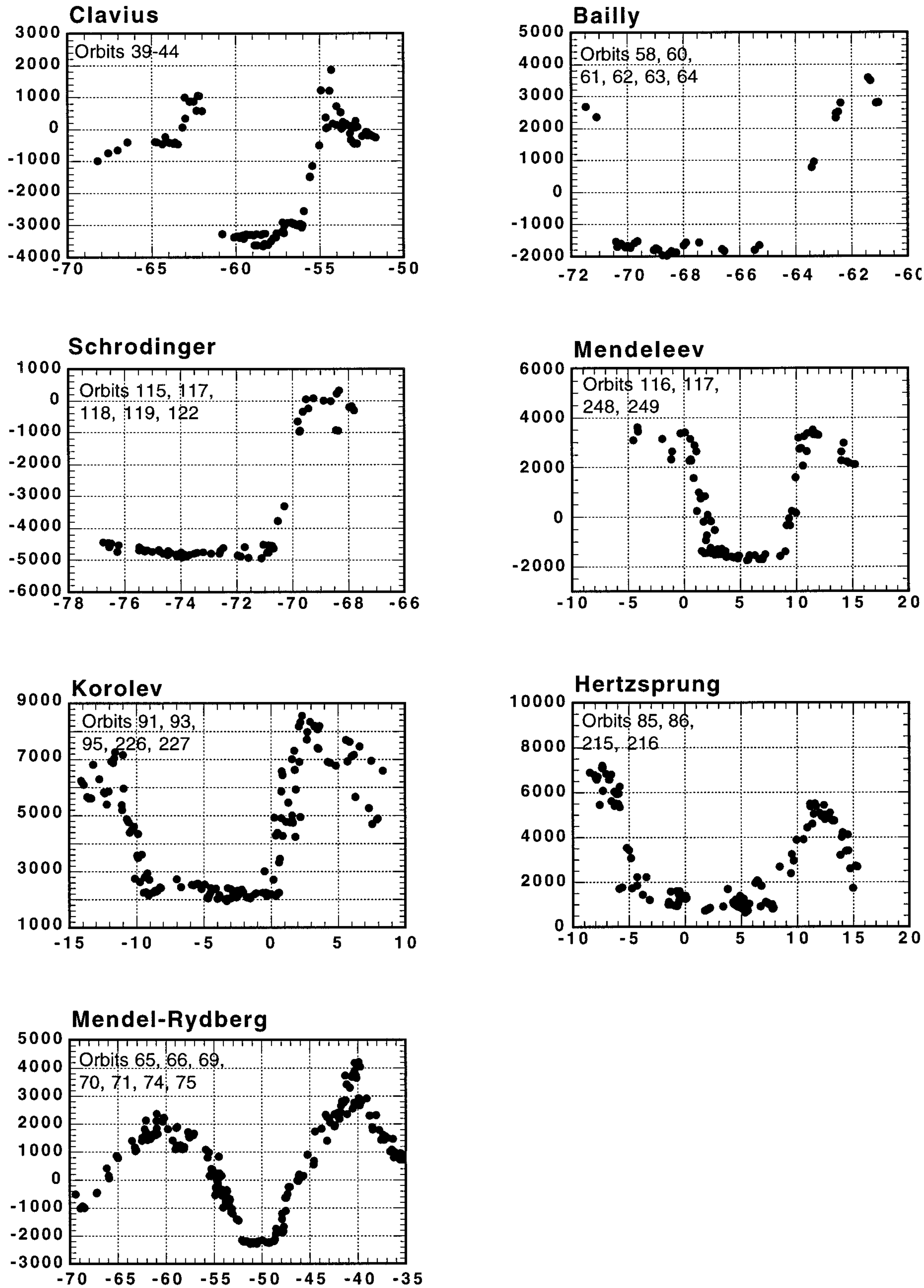

FIG. 4. LIDAR profiles of elevation (*m*) vs latitude over seven basins that define the *d*/*D* relation. Each profile is a compilation of data points from several orbital passes that were corrected to show the rim and floor at latitudes consistent with a pass over the center of the basin. The three largest basins show a statistically significant elevation difference between the north and south rims (see text for discussion).

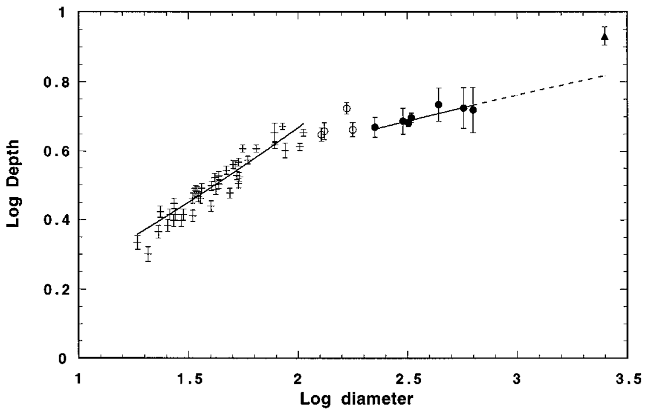

FIG. 5. $\log_{10}$(depth) versus $\log_{10}$(diameter) for complex craters (+) taken from LTOs and LIDAR data, transitional craters (open circles), and basins (solid circles), showing error bars for depth. The linear fit to the complex craters matches that of Pike (1974) and the fit to the basins is defined in the text. The South Pole–Aitken basin is denoted by a solid triangle and does not follow the depth/diameter relationship for basins.

The depths of the seven basins in Fig. 4 are plotted in Fig. 5 together with the freshest complex craters measured from LTOs (Pike 1976) and LIDAR data. The four complex craters that show floor roughening are considered as transitional (see Table I) and are denoted with a separate symbol. For completeness, we considered fits to the data using a single line, a curve, two lines (complex and basins), and two lines where the fit to the basins included three of the transitional craters (the possible ring of peaks in Hausen is not well developed). Using the F test for significance, it was found that fitting with one line gives the largest errors. Fitting with a curve is statistically better than with two lines; however, the F test does not account for a priori information about the data. The existence of a morphologic transition in the impact structures separates the data into two populations–complex craters and basins. Because data for simple and complex craters have been fit with a power law relation to each population instead of a curve to the full set of data (Pike 1974), the data for basins are treated in a similar manner. Further support for using two lines to fit the data comes from the distribution of data about the curve fit. Despite the better statistical fit to a curve, five of the seven basins fall below the best fit. Considering the transition in morphology, the distribution of basin data points about the curve fit, and the utility of presenting information in the same format as the data from Pike (1974), we concluded that the data should be fit by a power law relation for the separate populations of complex craters and basins as shown in Fig. 5.

We found that the depth of a basin changes with increasing diameter as

$$\log_{10}(d) = 0.41 \times [\log_{10}(D)]^{0.57}, \qquad (1)$$

where d is the depth in kilometers and D is the diameter in kilometers of the basin. We note that the fits to two lines with and without inclusion of the transitional craters are not significantly different.

Spudis and Adkins (1996) also measured selected lunar basin depths and reported a depth/diameter ratio similar to that of complex craters, but they excluded from consideration basins that fell below that trend on the basis of probable mare lava infilling. However, none of the basins on which our relationship is based contain significant mare fill at their centers. In addition, we note that basins measured in the Spudis and Atkins (1996) study that were also used to define our d/D trend for basins (Hertzprung, Korolev, Mendel-Rydberg, Mendeleev) in fact fall closer to our trend than to Pike's complex crater trend.

DISCUSSION

The depth/diameter curve of Pike (1974) showed a distinct inflection at the transition from simple to complex craters, but the lack of data points for large craters and basins prevented definitive discussions of what effect, if any, the complex crater to basin transition has on the relative depth of a crater. With the addition of new basin depths measured in this study, the d/D plot (Fig. 3) clearly shows a second break in slope over the diameter range of 100–200 km. This corresponds to diameters over which the transition from complex crater to basin morphology is observed (Stuart-Alexander and Howard 1970, Howard 1974, Head 1977, Wilhelms 1987, Melosh 1989, Spudis 1993). By comparing the slope of the d/D curve for basins with that for complex craters, it is possible to begin considering basin depths in the context of basin formation and modification mechanisms.

Basin Morphology and Ring Formation

The basins on which we focus in this analysis have diameters greater than 200 km; however, the morphologic evolution to basin may begin in craters with diameters as small as 50 km (Hale and Grieve 1982). With increasing diameters in complex craters, the central peaks transition into peak-rings, resulting in a reduction in depth of these transitional craters with respect to the d/D relationship for complex craters. It has been suggested that the transition to peak-rings is due to the collapse of large central peaks (Hale and Grieve 1982), gravitational instability of a large rebound (Croft 1981), or interaction of the transient cavity with the lunar Moho (Williams and Greeley 1997). A further increase in diameter is characterized by the appearance of additional rings consisting of structurally uplifted crust (Spudis 1993) and normal faults or scarps (Howard *et al.* 1974, McKinnon and Melosh 1980), making a continuous transition from complex crater to multiring basin (Croft 1981).

Spudis (1993) has combined several models for basin formation into a general scenario. After penetration of the initial cavity reaches its maximum depth, the basin floor undergoes rapid upward rebound due to the negative load of the initial cavity (Melosh 1989, Spudis 1993). Also, during this time, crustal material is fluidized due to the high energy of the impact (Melosh 1979, 1983) and moves upward above the uplifting mantle. It is in the subsequent short-term modification stage, which may last several minutes or longer, that gravitational and elastic forces become important (Croft 1981). During this time, mantle material uplifted during rebound reaches its maximum height and collapses due to gravitational instability. The motions of the upper crustal material together with collapse of the mantle rebound result in a basin floor which is gravitationally stable and relatively shallow (Melosh 1989).

Moving out from basin center, the collapse of structurally uplifted crustal material produces inner rings to the interior of the terrace zone (Melosh 1989, Spudis 1993). These rings are closest to basin center and show symmetric profiles, appearing as rounded mountains (Melosh 1989). At greater radial distances, rings are formed by dynamic collapse along inward dipping normal faults (Croft 1981) and have asymmetric profiles (Melosh 1989). There is some debate over how these faults are formed, with possibilities including megaterrace-forming collapse due to gravity (Head 1974, 1977, Croft 1981) or stresses caused by asthenospheric flow (Melosh and McKinnon 1978, Melosh 1989).

The identification of pseudotachylytes (frictional melt remnants) in the Sudbury impact feature has been cited as evidence that basin rings which formed in terrestrial impact structures represent remnants of large displacement fault zones (Spray and Thompson 1995). Formation of the pseudotacylyte zones as localizations of deformational energy dissipation suggests a large displacement which has been estimated at approximately 1 km at a depth of 5 km (Melosh 1995). It is also possible that the original displacements of faults comprising the outer rings of lunar basins may decrease shortly after their formation due to gravitational modification, contributing to the overall flattening of the basins (Croft 1981).

The occurrence of a second inflection in the depth/diameter curve over the diameter range of the morphologic transition from central peak craters to peak-ring basins suggests that the mechanisms which influence the transition from craters to basins also decrease the depth/diameter ratio with respect to that for complex craters. Possible complementary processes that contribute to relative shallowing of the depression include rebound and collapse of the transient cavity (Croft 1981), concentric faulting that causes rings characterized by normal faults (Head 1974, 1977, Croft 1981, Melosh and McKinnon 1978, Melosh 1989), and interaction of the transient cavity with the lunar Moho (Williams and Greeley 1997). Our observations are consistent with the magnitudes of these effects increasing with crater diameter.

Modification Mechanisms

Crater modification processes need to be considered as possible contributors to the decrease in relative depth. These include rim and floor degradation due to subsequent cratering, ejecta infilling, and viscous relaxation.

Degradation due to subsequent impacts can greatly reduce the topography of a crater. However, although there is evidence of rim and floor degradation in most lunar craters, such modification is minor in the freshest-appearing structures (Malin and Dzurisin 1977, Settle and Head 1977). Basins that have been visibly modified by large, subsequent impacts were excluded from our determination of the depth/diameter relation.

A more subdued form of modification is ejecta infilling. Those craters and basins that have undergone substantial infilling fall noticeably below the depth/diameter curve for well-preserved craters and basins. Although Cayley-type plains material thickness has been estimated at ~200 m (Hodges *et al.* 1973), it is not possible to measure accurately ejecta in the basins with present data. In most cases, ejecta thicknesses appear to be less than the error bars associated with the basin depth measurements.

Viscous relaxation of basin topography is possibly another important long-term modification process and is expected to manifest itself in the form of shallowed depths, possible domed basin floors, and associated fracturing (Solomon *et al.* 1982, Melosh 1989). For a Moon with a spatially homogeneous lithospheric thermal structure, the basins most likely to exhibit evidence for viscous degradation of topography are the largest, oldest structures. Solomon *et al.* (1982) quantitatively explored how the thermal and rheological condition of the lunar lithosphere at the time of pre-Nectarian impacts could result in greater viscous relaxation of those impact structures over geologic time as compared to younger basins, so these basins have been excluded from this analysis.

Interpretation

The most straightforward interpretation of the second break in slope of the d/D relation is that it indicates increased shallowing of crater depth relative to diameter due to the mechanisms associated with the morphologic transition from central peak craters to peak-ring basins. Long-term modification is quite likely to have reduced the depths of most lunar craters, and in fact we believe that the d/D relationship that we obtain underestimates fresh basin depths. However, we note that it would indeed be unusual if any of the crater modification mechanisms resulted in preferential shallowing of structures with diameters at the complex crater to basin transition and larger, i.e., producing an inflection in the d/D relationship. We consider it more likely that the inflection in the depth/diameter curve reported in this study is indicative of the fundamental processes that produce characteristic impact basin morphology.

South Pole-Aitken Basin

Clementine altimetry has shown that South Pole–Aitken is the largest and deepest impact basin in the Solar System (Spudis *et al.* 1994, Zuber *et al.* 1994), but how this ancient basin has maintained significant depth over geologic time has yet to be satisfactorily explained. While this basin is not treated in detail here, it should be noted that its depth is significantly greater than would be predicted by the depth/diameter relationship for lunar basins (Fig. 5). Because the diameter of the South Pole–Aitken basin exceeds the radius of the Moon, factors other than gravity and target properties, such as membrane stresses (R. J. Phillips, pers. commun. 1995) or impact angle (Schultz 1997), may have played a role in controlling the preserved depth of the basin. Further quantitative analysis of the significance of the depth of the South Pole–Aitken basin is warranted.

Orientale Basin

The Orientale basin has been cited as an example of a typical multiring basin (Stuart-Alexander and Howard 1970, Hartmann and Wood 1971, Head 1974, Solomon *et al.* 1982, Spudis 1993). Pre-Clementine topography of Orientale was derived from limb profiles (Watts 1963) as well as landmark elevations (Head *et al.* 1981). Until recently, data existed for only the eastern half of the basin (the part observable at the lunar limb from Earth) and it was necessarily assumed that this topography was characteristic of the rest of the basin (cf. Head 1982). Although there has been considerable debate about which ring represents the rim of the transient cavity (Baldwin 1972, Head 1974, Moore *et al.* 1974, Melosh 1980), the Cordillera mountains, which are defined by a 2- to 7-km-high scarp (Melosh 1980) on the eastern side of Orientale, correspond to the main topographic rim of the basin (Croft 1981, Wilhelms 1987). Previously calculated thicknesses of the small mare patch in Orientale range from <1 km (Head 1974, Greeley 1976, Scott *et al.* 1977) to 1.7 km (Solomon and Head 1980), and using the assumed topography of the basin, the Cordillera mountains were measured to rise approximately 8 km above the mare surface (Head 1982). Adding the mare thickness to the height of the Cordillera mountains gives a pre-mare basin depth of 9–10.

With Clementine topographic coverage of the entire basin, including the western rim which previously lacked coverage, Orientale can now be studied in a uniform manner. The Clementine topography of the basin and surrounding region, shown in Fig. 6a, reveals significant topographic complexity. Of particular significance is the fact that Orientale lies at the boundary between mare and highlands with a variation in regional topography of approximately 6 km from 1000 km east of basin center to 1000 km west of basin center (Fig. 6b). This corresponds to a regional slope of 0.17° over this baseline, but the topographic change is obscured by the basin and may not be smoothly varying. The regional topography is also affected by the Mendel-Rydberg basin to the south, the South Pole–Aitken basin to the southwest, and some of the highest and roughest topography on the Moon to the west and northwest. Orientale is also in a location where the crust is relatively thin (~60 km) exterior to the eastern rim and thick (~80 km) outside of the western rim (Neumann *et al.* 1996).

It is clear that the E–W variation in topography, the neighboring topographic highs and lows, and the variation in crustal thickness must have affected the topographic expression of Orientale. Because regional factors have had a demonstrable effect on the morphology of Orientale, an average of rim heights around the basin would not give a useful result unless the contributions of the outside influences could be taken into account. Therefore, the topographic complexity of the Orientale basin warrants particular caution in the interpretation of its depth.

CALCULATION OF MARE THICKNESSES

The thicknesses of maria in the lunar basins can be used to estimate the volume of mare basalt produced on the Moon (Head 1974, Solomon and Head 1980, Head 1982, Antonenko and Head 1995, Yingst and Head 1995, Spudis and Adkins 1996, Williams and Zuber 1996). Such estimates are relevant to discussions of magma generation and ascent to the lunar surface (Head and Wilson 1992, Antonenko and Head 1995, Yingst and Head 1995, Hess and Parmentier 1995) and can lead to implications for the lunar thermal state at the time of mare volcanism (Solomon *et al.* 1982, Bratt *et al.* 1985a, Alley and Parmentier 1996, Solomon and Simons 1996). In addition, the thicknesses of maria in the major basins are required for stress calculations used to estimate lunar lithospheric thicknesses (Melosh 1976, 1978, Comer *et al.* 1979, Solomon and Head 1980, Pullan and Lambeck 1981, Williams *et al.* 1995). Investigations into the structure of the lunar crust in the regions around mare basins (Spudis *et al.* 1994, Zuber *et al.* 1994, Neumann *et al.* 1996, Williams *et al.* 1995, Kiefer and Dodge 1996, von Frese *et al.* 1996, Wieczorek and Phillips 1997) also benefit from mare thickness estimates, because the thicknesses must be known in order to subtract the effect of high-density mare material from the Bouguer gravity, i.e., the gravity signal remaining after correction for the gravitational attraction of surface topography.

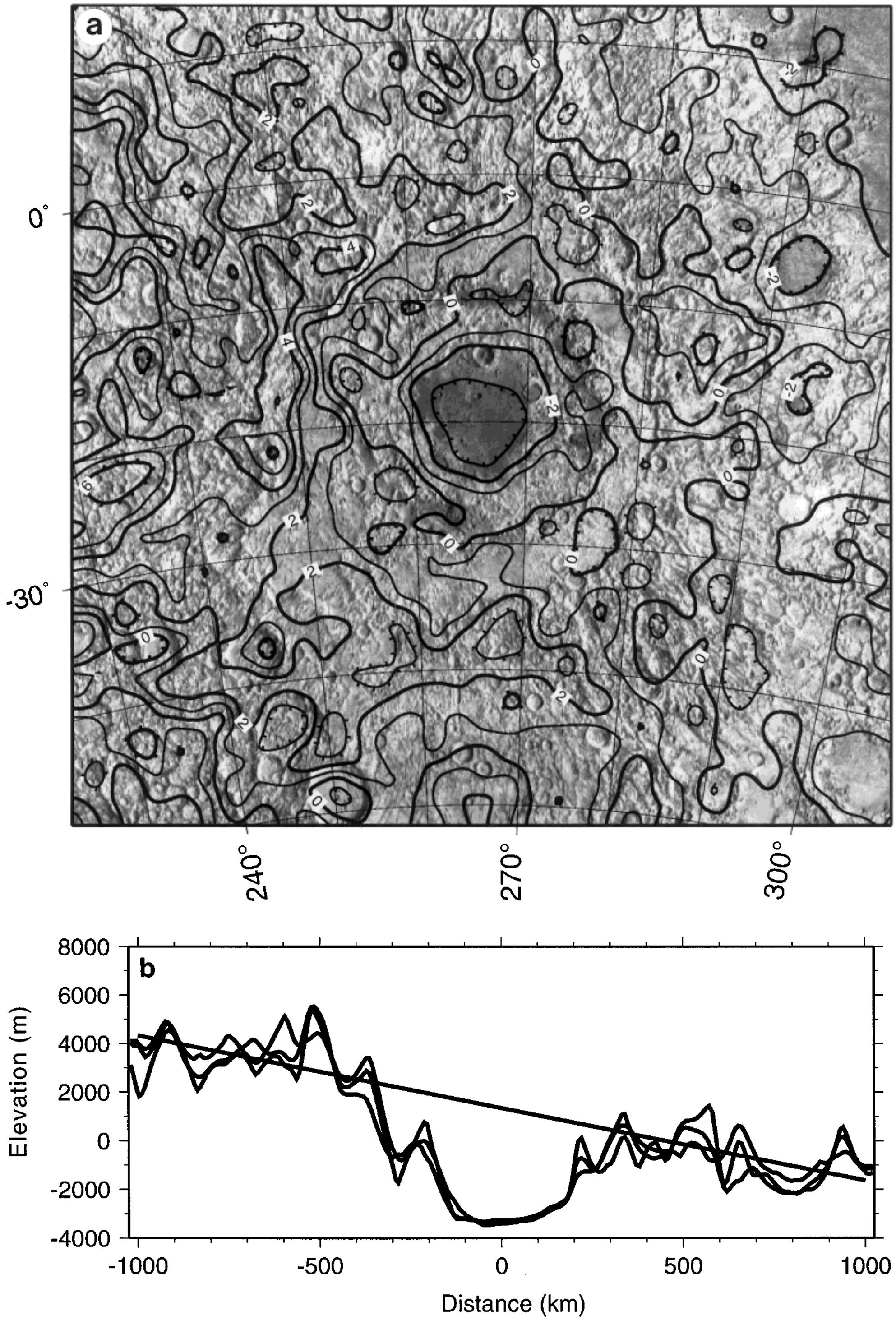

FIG. 6. (a) Contour map of the region surrounding the Orientale basin (19°S, 265°E, D = 930 km). Topography around the basin varies by as much as 10 km. (b) Three west–east topographic profiles taken from a 50-km-wide track centered at 20° south latitude plotted together with a regional, linear trend calculated for the same track. The west–east tracks were taken from a global grid of Clementine topography produced by Smith *et al.* (1997).

Mare thicknesses have previously been estimated by assuming that partially flooded craters which formed prior to mare filling follow the depth/diameter relationship of Pike (1974) and by measuring the depth to the mare in the crater (DeHon 1974, 1977, 1979, DeHon and Waskom 1976). It was noted by Hörz (1978), however, that the craters may have been more degraded than DeHon assumed, resulting in a decrease in mare thickness by as much as a factor of two. In addition, Head (1982) noted that the number of craters used as data points in DeHon's method is small due to the reduction in cratering flux and that the thicker mare in the basin centers totally buried shallow craters. Recently, craters which excavated through the basalt to expose crustal material have been used to calculate independent mare thicknesses (Budney and Lucey 1996, Gillis *et al.* 1997). While all these methods result in thicknesses for the outer edges of the mare regions, they cannot be used to estimate the thicknesses at the centers of the maria. Thicknesses at mare basin centers were, however, estimated by calculating the amount of mare fill required to produce the gravity highs over the mascons (Comer *et al.* 1979, Solomon and Head 1980). These studies resulted in thickness values that could be used in stress calculations, but the gravity anomaly magnitudes were limited by Apollo-era coverage and it was assumed that the entire Bouguer gravity anomaly was due to the mare load. Another method was employed by Head (1982) to study the geometries, thicknesses, and volumes of the maria using Orientale as an example of a relatively unfilled young basin. He concluded that a totally flooded Orientale basin (or any other young basin of the same diameter, assuming Orientale's topography is representative) would have a mare thickness of approximately 9 km at its center. Although Head (1982) arrives at a mare thickness value for a totally flooded multiring basin, he notes that reconstructing the sub-volcanic topography of a basin is the major difficulty in establishing mare thicknesses.

The Clementine topography data now make it possible to use an alternative approach for measuring the mare thicknesses in the major basins. By assuming that the eight large mare-flooded basins have undergone the same amount of degradation due to impacts as those that define the d/D relation, the depths of the basins prior to mare filling can be predicted by fitting their diameters to the d/D relationship for basins. The thicknesses of the maria at the centers of the basins can then be calculated by subtracting the depth to the mare surface from the predicted depth if no mare were present. Figure 7 shows the measured depth to the mare surface and the predicted basin depth plotted with lines defining the power law relations for complex craters and basins. The difference between the predicted basin depth and the measured depth to the mare surface is the estimated mare thickness.

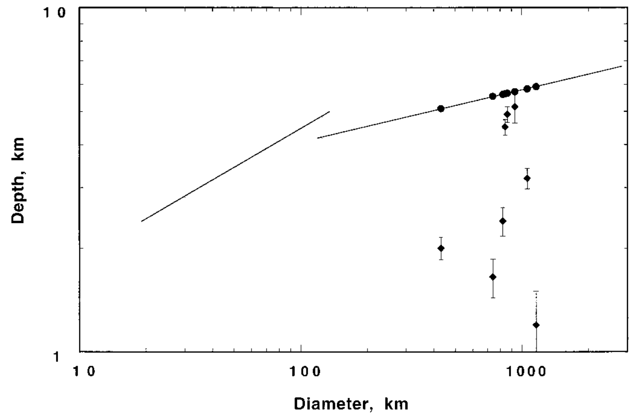

FIG. 7. Depths from rim crest to mare surface for eight mare basins (solid diamonds) plotted against lines defining the depth/diameter relations for complex craters and basins. The predicted depths for the basins if they did not contain mare are plotted as solid circles. The estimated mare thickness is the difference between the two values after taking subsidence due to mare loading into account.

Because the lunar lithosphere must have been characterized by a finite flexural strength (e.g., Melosh 1978, Solomon and Head 1980), the subsidence due to the high density mare material is included in the calculations. Also, the mare thicknesses that would result from using the fit both with and without the transitional craters were calculated, but only a slight difference in mare thicknesses existed between the two fits. Thus, the power law fit to the seven basins was used to find the final mare thicknesses.

Table II lists the diameter, predicted unfilled depth using the d/D relationship, depth to mare surface, resulting mare thickness, mare thickness after adjusting for subsidence, and associated errors for the eight large mare basins considered. The values for elastic lithospheric thickness used in the calculations of subsidence are taken from Neumann and Zuber (1996) and are also listed in Table II. It should be noted that our values for mare thickness represent lower limits because the depths of the basins used to define the d/D relationship may have been decreased by viscous effects, infilling by ejecta, or rim degradation. The errors associated with the thicknesses represent the root sum squared values of measurement errors for depth to mare surface and the difference in predicted unfilled basin depth using the two depth/diameter relations for lunar basins (with and without transitional craters). A correction for the uncertainty in the assumed elastic lithospheric thicknesses is also included.

Table III compares the mare thicknesses calculated in this study with those estimated by Solomon and Head (1980) using gravity analysis and by others using the partially buried crater method (DeHon 1974, 1977, 1979, DeHon and Waskom 1976). Values from calculations of the mare thickness necessary to result in the Apollo-era gravity anomaly of the mascon (Solomon and Head 1980) are

TABLE II
Predicted Depths of Mare Basins Prior to Mare Filling and Resulting Mare Thickness Estimates

Basin	Diameter[a]	Predicted depth	Depth to mare	Thickness	Adjusted	Error	*T*
Grimaldi	430	5.10	2.00 ± .15	3.10	3.46	0.17	75
Serenitatis	740	5.53	1.65 ± .21	3.88	4.30	0.33	90
Humorum	820	5.61	2.40 ± .23	3.21	3.61	0.38	60
Smythii	840	5.63	4.50 ± .23	1.13	1.28	0.38	50
Nectaris	860	5.65	4.90 ± .25	0.75	0.84	0.40	55
Orientale	930	5.71	5.15 ± .52	0.56	0.63	0.62	65
Crisium	1060	5.82	3.20 ± .22	2.62	2.94	0.45	65
Imbrium	1160	5.90	1.20 ± .30	4.70	5.24	0.52	60

Note. All values are given in units of km.
[a] Diameters of main topographic rings from Wilhelms (1987).

generally larger than the values estimated in this study. Because Solomon and Head assumed that the entire gravity signal was due to the mare load and did not allow for a component due to an upwarped plug of mantle material (Wise and Yates 1970, Bratt *et al*. 1985a, Neumann *et al*. 1996, Williams *et al*. 1995), their values are most likely overestimates of mare thickness. For Mare Humorum, the technique used here yields a thickness slightly greater than determined by Solomon and Head. The larger value estimated here could be due to the fact that analyses of Apollo-era gravity sometimes underestimated the amplitude of the peak anomaly (Lemoine *et al.* 1997).

Conversely, the mare thicknesses measured using partially buried craters are mostly less than those calculated in this study. It is likely that the difference is due to the distribution of partially filled craters preventing measurement of mare thickness at the center of the basin. In two cases (Nectaris and Crisium), our method resulted in thinner mare than that of DeHon, possibly due to DeHon's assumption that the flooded craters had not undergone degradation prior to mare filling (Hörz 1978).

TABLE III
Mare Thicknesses Estimated in This Study Compared to Previous Estimates

Basin	This study	Solomon and Head (1980)	Flooded crater method[a]
Grimaldi	3.46 ± .17	3.6	0.5
Serenitatis	4.30 ± .33	8.5	3.5
Humorum	3.61 ± .38	2.7	2.5
Smythii	1.28 ± .38	4.5	0.5
Nectaris	0.84 ± .40	4.5	2.3
Orientale	0.63 ± .62	1.7	—
Crisium	2.94 ± .45	7.4	3–4
Imbrium	5.24 ± .52	9.2	1.5

Note. All values are given in units of km.
[a] From DeHon (1974, 1979) and DeHon and Waskom (1976).

As implicitly assumed in crater filling studies, our method assumes that the sub-volcanic topography in the mascon basins is similar to that in the best preserved, unfilled basins and uses that assumption to arrive at the mare thicknesses at the centers of the major basins. The thicknesses of maria presented here are less than would be predicted by complete flooding of the Orientale basin (Head 1982), but atypical influences on the topography of Orientale have already been discussed and support the warning by Head (1982) that caution should be exercised in using Orientale as an example of a typical basin. Head (1982) also noted that Orientale, Nectaris, and Smythii have undergone less filling than the other mascon basins, and our results agree with that observation (see Table III).

We consider these measurements to be complementary to those of previous analyses and believe they are particularly valuable in refining the uncertainty associated with estimates of mare thicknesses. The values for mare thickness estimated in this study have been and are currently being used to remove the attraction of the high density mare material from the lunar gravity field in order to investigate the subsurface structure and compensation states of lunar basins (Neumann and Zuber 1996, Neumann *et al.* 1996, Williams *et al.* 1995).

SUMMARY

The near-global coverage of lunar topography provided by the Clementine LIDAR has enabled depth measurements for a number of large basins. Due to the limited coverage and, to a lesser extent, accuracy of pre-Clementine topographic data for the Moon, it was not previously possible to measure accurately basin depths. Using the corrected Clementine profile data in combination with photographic images, we have shown that the LIDAR instrument detected the rims of 29 large impact structures well enough to measure their depths. These depths were plotted together with data for simple and complex craters measured from LTOs (Pike 1976) to produce a depth/diameter plot that includes lunar basins. The plot reveals a second break in slope (i.e., in addition to the one previously noted at the simple to complex crater transition by Pike (1974)) that coincides with the morphologic transition from complex craters to basins. A linear fit to the seven best preserved basins shows that lunar basins obey a power law increase in depth with increasing diameter where the log linear slope of the best-fit line is less than that for complex craters. The decrease in the slope of the fit agrees with a prediction of a further decrease in the d/D ratio with increasing basin diameter (Melosh 1989). On the basis of a qualitative evaluation of probable causes, we interpret the second inflection in the depth/diameter relationship as being due to a short-term modification mechanism that influenced fundamental crater morphology—most likely related to mechanisms that cause the transition from crater to basin.

Because ancient lunar basins possess information about the thermal setting in which they formed, their depths can be used as constraints on the thermal conditions of the young Moon. Significant viscous relaxation effects are not apparent in the basins measured in this analysis, suggesting that the thermal and mechanical properties of the lithosphere required for such relaxation were not uniformly present over the Moon following basin formation. However, further detailed studies of viscous relaxation of basin topography using basin shapes from Clementine data are warranted for a better understanding of that process.

We have also used the depth/diameter relation for basins to predict the sub-volcanic depths of the major mare-flooded basins. These new values generally fall between previous estimates from gravity analysis that likely overestimated thicknesses and from flooded crater studies that may have underestimated them.

Unlike previous estimates of the d/D relationship for simple and complex craters for which large statistical samples could be amassed, the relation for basins is based on a limited pool of observations. However, the consistency of the data set, in combination with the correspondence of the second break in slope to the complex crater to basin transition, indicates that the basin depths measured from Clementine topographic profiles are providing a fundamental piece of information about basin structural form and not only late stage modificational history. Our analysis has also elucidated the atypical topography of the Orientale basin as well as the deep, largely unrelaxed South Pole–Aitken basin that does not follow the depth/diameter relationship. It has been noted that knowledge of basin mechanics decreases with increasing basin diameter (Melosh 1980). This investigation of how basin depths vary with increasing size, and the deviations from established relationships, is a step toward gaining a better understanding of the process of basin formation and its implications for the thermal and physical properties of the early Moon.

ACKNOWLEDGMENTS

We are thankful to H. J. Melosh and P. D. Spudis for constructive reviews, and we appreciate helpful discussions with G. Neumann, M. Cintala, P. Spudis, and K. McCormick. We also thank G. Neumann for drafting several figures and B. Campbell for access to and assistance with the LTOs. This work was supported by grants from the NASA Planetary Geology and Geophysics Program and the NASA Lunar and Asteroid Data Analysis Program.

REFERENCES

Alley, K. M., and E. M. Parmentier 1996. Thermal convection in an initially compositionally stratified fluid heated from below: Application to a model for the evolution of the Moon. *Lunar Planet. Sci. Conf. 27th,* 21–22.

Antonenko, I., and J. W. Head 1995. Estimates of cryptomare thickness and volume in Schiller–Schickard, Mare Humorum and Oceanus Procellarum areas. *Lunar Planet. Sci. Conf. 26th,* 47–48.

Baldwin, R. B. 1971. The nature of isostasy on the Moon. *Phys. Earth Planet. Int.* **4,** 167–179.

Baldwin, R. B. 1972. The tsunami model of the origin of ring structures concentric with large lunar craters. *Phys. Earth Planet. Int.* **6,** 327–339.

Bratt, S. R., S. C. Solomon, J. W. Head, and C. H. Thurber 1985a. The deep structure of lunar basins: Implications for basin formation and modification. *J. Geophys. Res.* **90,** 3049–3064.

Bratt, S. R., S. C. Solomon, and J. W. Head 1985b. The evolution of impact basins: Cooling, subsidence, and thermal stress. *J. Geophys. Res.* **90,** 12,415–12,433.

Budney, C. J., and P. G. Lucey 1996. Basalt thickness in Mare Humorum: New method and results, *Lunar Planet. Sci. Conf. 27th,* 179–180.

Cole, T. D., M. T. Boise, A. S. El-Dinary, A. F. Cheng, M. T. Zuber, and D. E. Smith 1997. The Near Earth Asteroid Rendezvous Laser Altimeter *Space Sci. Rev.*, in press.

Comer, R. P., S. C. Solomon, and J. W. Head 1979. Elastic lithosphere thickness on the Moon from mare tectonic features: A formal inversion. *Proc. Lunar Planet. Sci. Conf. 10th,* 2441–2463.

Croft, S. K. 1981. The modification stage of basin formation: Conditions of ring formation. *Proc. Lunar Planet. Sci. Conf. 12th,* 227–257.

DeHon, R. A. 1974. Thickness of mare material in the Tranquillitatis and Nectaris basins. *Proc. 5th Lunar Conf.* **1,** 53–59.

DeHon, R. A. 1977. Mare Humorum and Mare Nubium: Basalt thickness and basin-forming history. *Proc. Lunar Planet. Sci. Conf. 8th,* 633–641.

DeHon, R. A. 1979. Thickness of western mare basalts. *Proc. Lunar Planet. Sci. Conf. 10th,* 2935–2955.

DeHon, R. A., and J. D. Waskom 1976. Geologic structure of the eastern mare basins. *Proc. Lunar Planet. Sci. Conf. 7th,* 2729–2746.

Dence, M. R. 1971. Impact melts. *J. Geophys. Res.* **76,** 5552–5565.

Garvin, J., J. B. Blair, and J. L. Bufton 1997. The Shuttle Laser Altimeter (SLA-01) experiment: Topographic remote sensing of planet Earth. *Science*, submitted.

Gault, D. E., and E. D. Heitowit 1963. The partition of energy for hypervelocity impact craters formed in rock. *Proc. 6th Hypervelocity Impact Symp.* **2,** 419–456.

Gault, D. E., J. E. Guest, J. B. Murray, J. B. Dzurisin, and M. C. Malin 1975. Some comparisons of impact craters on Mercury and the Moon. *J. Geophys. Res.* **80,** 2444–2460.

Gillis, J. J., P. D. Spudis, and D. B. J. Bussey 1997. The geology of Smythii and Mariginis basins using integrated remote sensing techniques: A look at what's around the corner. *Proc. Lunar Planet. Sci. Conf. 28th,* 419–420.

Greeley, R. 1976. Modes of emplacement of basalt terrains and an analysis of mare volcanism in the Orientale basin. *Proc. Lunar Planet. Sci. Conf. 7th,* 2747–2749.

Hale, W. S., and R. A. F. Grieve 1982. Volumetric analysis of complex lunar craters: Implications for basin rim formation. *J. Geophys. Res.* **87,** A65–A76.

Hall, J. L., S. C. Solomon, and J. W. Head 1981. Lunar floor-fractured craters: Evidence for viscous relaxation of crater topography. *J. Geophys. Res.* **86,** 9537–9552.

Hartmann, W. K., and C. A. Wood 1971. Moon: Origin and evolution of multiring basins. *The Moon* **3,** 3–78.

Head, J. W. 1974. Orientale multi-ringed basin interior and implications for the petrogenesis of lunar highland samples. *Moon* **11,** 327–356.

Head, J. W. 1976. The significance of substrate characteristics in determining morphology and morphometry of lunar craters. *Proc. Lunar Planet. Sci. Conf. 7th,* 2913–2929.

Head, J. W. 1977. Origin of outer rings in lunar multi-ring basins: Evidence for morphology and ring spacing. In *Impact and Explosion Cratering* (D. J. Roddy, R. O. Peppin, and R. B. Merrill, Ed.), pp. 563–573, Pergamon, NY.

Head, J. W. 1982. Lava flooding of ancient planetary crusts: Geometry, thickness, and volumes of flooded lunar impact basins. *Moon and Planets* **26,** 61–88.

Head, J. W., E. Robinson, and R. Phillips 1981. Topography of the Orientale basin. *Proc. Lunar Planet. Sci. Conf. 12th,* 421–423.

Head, J. W., and L. Wilson 1992. Lunar mare volcanism: Stratigraphy, eruption conditions, and the evolution of secondary crusts. *Geochim. Cosmochim. Acta* **56,** 2155–2175.

Hess, P. H., and E. M. Parmentier 1995. A model for the thermal and chemical evolution of the Moon's interior: Implications for the onset of mare volcanism. *Earth Planet. Sci. Lett.* **134,** 501–514.

Hodges, C. A., W. R. Muehlberger, and G. E. Ulrich 1973. Geologic setting of Apollo 16. *Proc. 4th Lunar Sci. Conf.* **1,** 1–25.

Hörz, F. 1978. How thick are lunar mare basalts? *Proc. Lunar Planet. Sci. Conf. 9th,* 3311–3331.

Howard, K. A. 1974. Fresh lunar impact craters: Review of variations with size. *Proc. 5th Lunar Sci. Conf.* **1,** 61–69.

Howard, K. A., D. E. Wilhelms, and D. H. Scott 1974. Lunar basin formation and highland stratigraphy. *Rev. Geophys. Space Phys.* **12,** 309–327.

Johnson, T. V., and T. R. McGetchin 1973. Topography on satellite surfaces and the shape of asteroids. *Icarus* **18,** 612–620.

Kaula, W. M. 1979. Thermal evolution of Earth and Moon by growing planetesimal impacts. *J. Geophys. Res.* **84,** 999–1008.

Kaula, W. M., M. J. Drake, and J. W. Head 1986. The Moon. In *Satellites* (J. A. Burns and M. S. Matthews, Ed.), pp. 581–629, Univ. of Arizona Press, Tucson.

Kiefer, W. S., and M. C. Dodge 1996. Uncompensated mare basalts as a model for lunar mascons, *Proc. Lunar Planet. Sci. Conf. 27th,* 665–666.

Lemoine, F. G., D. E. Smith, M. T. Zuber, D. D. Rowlands, and G. A. Neumann 1995. Results from the Clementine lunar geodesy investigation. *Astrodynamics* **90,** 201–223.

Lemoine, F. G., D. E. Smith, M. T. Zuber, G. A. Neumann, and D. D. Rowlands 1997. A 70th degree and order lunar gravity model from Clementine and historical data. *J. Geophys. Res.* **102,** 16,339–16,359.

Lucey, P. G., G. J. Taylor, and E. Malaret 1995. Abundance and distribution of iron on the Moon. *Science* **268,** 1150–1153.

Malin, M. C., and D. Dzurisin 1977. Landform degradation on Mercury, the Moon, and Mars: Evidence from crater depth/diameter relationships. *J. Geophys. Res.* **82,** 376–388.

Malin, M. C., and D. Dzurisin 1978. Modification of fresh crater landforms: Evidence from the Moon and Mercury. *J. Geophys. Res.* **83,** 233–243.

McEwen, A. S., and E. M Shoemaker 1995. Two classes of impact basins on the Moon. *Proc. Lunar Planet. Sci. Conf. 26th,* 935–936.

McGetchin, T. R., M. Settle, and J. W. Head 1973. Radial thickness variation in impact crater ejecta: Implications for lunar basin deposits. *Earth Planet. Sci. Lett.* **20,** 226–236.

McKinnon, W. B. 1978. An investigation into the role of plastic failure in crater modification. *Proc. Lunar Planet. Sci Conf. 9th,* 3965–3973.

McKinnon, W. B., and H. J. Melosh 1980. Evolution of planetary lithospheres: Evidence from multiringed structures on Ganymede and Callisto. *Icarus* **44,** 454–471.

Melosh, H. J. 1976. On the origin of fractures radial to lunar basins. *Proc. Lunar Planet. Sci. Conf. 7th,* 2967–2982.

Melosh, H. J. 1977. Crater modification by gravity: A mechanical analysis of slumping. In *Impact and Explosion Cratering* (D. J. Roddy, R. O. Pepin, and R. B. Merrill, Ed.), pp. 1245–1260. Pergamon, New York.

Melosh, H. J. 1978. The tectonics of mascon loading. *Proc. Lunar Planet. Sci. Conf. 9th,* 3513–3525.

Melosh, H. J. 1979. Acoustic fluidization: A new geologic process? *J. Geophys. Res.* **84,** 7513–7520.

Melosh, H. J. 1980. Cratering mechanics—Observational, experimental, and theoretical. *Ann. Rev. Earth Planet. Sci.* **8,** 65–93.

Melosh, H. J. 1982. A schematic model of crater modification by gravity. *J. Geophys. Res.* **87,** 371–380.

Melosh, H. J. 1983. Acoustic fluidization. *Am. Sci.* **71,** 158–165.

Melosh, H. J. 1989. *Impact Cratering: A Geologic Process*. Oxford Univ. Press, New York.

Melosh, H. J. 1995. Under the ringed basins. *Nature* **373,** 104–105.

Melosh, H. J., and W. B. McKinnon 1978. The mechanics of ringed basin formation. *Geophys. Res. Lett.* **5,** 985–988.

Moore, H. J., C. A. Hodges, and D. H. Scott 1974. Multiringed basins—Illustrated by Orientale and associated features. *Proc. Lunar Planet. Sci. Conf. 5th,* 71–100.

Neumann, G. A., and M. T. Zuber 1996. Coherence of lunar mare basins. *Proc. Lunar Planet. Sci. Conf. 27th,* 953–954.

Neumann, G. A., M. T. Zuber, D. E. Smith, and F. G. Lemoine 1996. The lunar crust: Global structure and signature of major basins. *J. Geophys. Res.* **101,** 16,841–16,863.

Nozette, S., P. L. Rustan, L. P. Plesance, D. M. Horan, P. Regeon, E. M. Shoemaker, P. D. Spudis, C. Acton, D. N. Baker, J. E. Blamont, B. J. Buratti, M. P. Corson, M. E. Davies, T. C. Duxbury, E. M. Eliason, B. M. Jakosky, J. F. Kordas, I. T. Lewis, C. L. Lichtenberg, P. G. Lucey, E. Malaret, M. A. Massie, J. H. Resnick, C. J. Rollins, H. S. Park, A. S. McEwen, R. E. Priest, C. M. Pieters, R. A. Reisse, M. S. Robinson, R. A. Simpson, D. E. Smith, T. C. Sorenson, R. W. Vorder Bruegge, and M. T. Zuber 1994. The Clementine mission to the Moon: Scientific overview. *Science* **266,** 1835–1839.

O'Keefe, J. D., and T. J. Ahrens 1979. The effect of gravity on impact crater excavation time and maximum depth: Comparison with experiment. *Proc. Lunar Planet. Sci. Conf. 10th,* 934–936.

Parmentier, E. M., and J. W. Head 1981. Viscous relaxation of impact craters on icy planetary surfaces: Determination of viscosity variation with depth. *Icarus* **47,** 100–111.

Passey, Q. R., and E. M. Shoemaker 1982. Craters and basins on Ganymede and Callisto: Morphological indicators of crustal evolution. In *Satellites of Jupiter* (D. Morrison and M. S. Matthews, Ed.), pp. 379–434, Univ. of Arizona Press, Tucson.

Pike, R. A. 1974. Depth/diameter relations of fresh lunar craters: Revision from spacecraft data. *Geophys. Res. Lett.* **1,** 291–294.

Pike, R. A. 1976. Crater dimensions from Apollo data and supplemental sources. *Moon* **15,** 463–477.

Pike, R. A. 1980. Formation of complex impact craters: Evidence from Mars and other planets. *Icarus* **43,** 1–19.

Pike, R. A. 1983. Comment on ''A schematic model of crater modification by gravity'' by H. J. Melosh. *J. Geophys. Res.* **88,** 2500–2504.

Pullan, S., and K. Lambeck 1981. Mascons and loading of the lunar lithosphere. *Proc. Lunar Planet. Sci. Conf. 12th,* 853–865.

Quaide, W. L., D. E. Gault, and R. A. Schmidt 1965. Gravitative effects on lunar impact structures. *Ann. NY Acad. Sci.* **123,** 563–572.

Safronov, V. S. 1972. *Evolution of the Protoplanetary Cloud and Formation of the Earth and Planets,* NASA Tech. Transl. TT F-677. Nauka, Moscow.

Schubert, G., T. Spohn, and R. T. Reynolds 1986. Thermal histories, compositions, and internal structures of the moons of the Solar System. In *Satellites*, (J. A. Burns and M. S. Matthews, Ed.), pp. 224–292, Univ. of Arizona Press, Tucson.

Schultz, P. H. 1997. Forming the South Pole-Aitken basin: The extreme games. *Proc. Lunar Planet. Sci. Conf. 28th,* 1259–1260.

Scott, D. H., J. F. McCauley, and M. N. West 1977. Geologic map of the west side of the moon. U.S. Geol. Survey Map I-1034.

Scott, R. F. 1967. Viscous flow of craters. *Icarus* **7,** 139–148.

Settle, M., and J. W. Head 1977. Radial variation of lunar crater rim topography. *Icarus* **31,** 123–135.

Settle, M., and J. W. Head 1979. The role of rim slumping in the modification of lunar impact craters. *J. Geophys. Res.* **84,** 3081–3096.

Smith, D. E., M. T. Zuber, G. A. Neumann, and F. G. Lemoine 1997. Topography of the Moon from the Clementine LIDAR. *J. Geophys. Res.* **102,** 1591–1611.

Solomon, S. C. 1978. The nature of isostasy on the Moon: How big a Pratt-fall for Airy models? *Proc. Lunar Planet. Sci. Conf. 9th,* 3499–3511.

Solomon, S. C. 1986. On the Early Thermal Evolution of the Moon. In *Origin of the Moon* (W. K. Hartmann, R. J. Phillips, and G. J. Taylor, Eds.), pp. 435–452. Lunar Planetary Institute, Houston.

Solomon, S. C., and J. W. Head 1979. Vertical movement in mare basins: Relation to mare emplacement, basin tectonics, and lunar thermal history. *J. Geophys. Res.* **84,** 1667–1682.

Solomon, S. C., and J. W. Head 1980. Lunar mascon basins: Lava filling, tectonics, and evolution of the lithosphere. *Rev. Geophys. Space Phys.* **18,** 107–141.

Solomon, S. C., R. P. Comer, and J. W. Head 1982. The evolution of impact basins: Viscous relaxation of topographic relief. *J. Geophys. Res.* **87,** 3975–3992.

Solomon, S. C., and M. Simons 1996. The isostatic state of the lunar highlands from spatio-spectral localization of global gravity, topography, and surface chemistry. *Proc. Lunar Planet. Sci. Conf. 27th,* 1245–1246.

Spray, J. G., and L. M. Thompson 1995. Friction melt distribution in a multiring impact basin. *Nature* **373,** 130–132.

Spudis, P. D. 1993. *The Geology of Multi-Ring Impact Basins: The Moon and Other Planets*. Cambridge Univ. Press, Cambridge.

Spudis, P. D. 1995. Clementine laser altimetry and multi-ring basins on the Moon. *Proc. Lunar Planet. Sci. Conf. 26th*, 1337–1338.

Spudis, P. D., R. A. Riesse, and J. J. Gillis 1994. Ancient multiring basins on the Moon revealed by Clementine laser altimetry. *Science* **266**, 1848–1851.

Spudis, P. D., and C. D. Adkins 1996. Morphometry of basins on the Moon: New results from Clementine laser altimetry. *Proc. Lunar Planet. Sci. Conf. 27th,* 1253–1254.

Stuart-Alexander, D. E., and K. A. Howard 1970. Lunar maria and circular basins—A review. *Icarus* **12,** 440–456.

von Frese, R. R. B., L. Tan, L. V. Potts, C. J. Merry, and J. D. Bossler 1996. Lunar crustal modeling of Mare Orientale from Clementine satellite observations. *Proc. Lunar Planet. Sci. Conf. 27th,* 1363–1364.

Watts, C. B. 1963. The marginal zone of the Moon. *Astron. Papers Am. Ephemer. Naut. Almanac* **17**.

Wieczorek, M. A., and R. J. Phillips 1997. The structure and compensation of the lunar highland crust, *J. Geophys. Res.* **102,** 10,933–10,943.

Wilhelms, D. E. 1987. *The Geologic History of the Moon*. U.S. Government Printing Office, Washington, DC.

Williams, K. K., G. A. Neumann, and M. T. Zuber 1995. Lunar mascon basins: Analysis of effective elastic thickness using gravity anomaly models. *Proc. Lunar Planet. Sci. Conf. 26th,* 1505–1506.

Williams, K. K., and M. T. Zuber 1996. Re-evaluation of mare thicknesses based on lunar crater depth/diameter relationships. *Proc. Lunar Planet. Sci. Conf. 27th,* 1441–1442.

Williams, K. K., and R. Greeley 1997. The effect of lunar crustal thickness on the morphologic transition from central peak to peak-ring craters. *Proc. Lunar Planet. Sci. Conf. 28th,* 1557–1558.

Wise, D. U., and M. T. Yates 1970. Mascons as structural relief on a lunar Moho. *J. Geophys. Res.* **75,** 261–268.

Wood, C. A., and J. W. Head 1976. Comparison of impact basins on Mercury, Mars and the Moon. *Proc. Lunar Planet. Sci. Conf. 7th,* 3629–3651.

Yingst, R. A., and J. W. Head 1995. Spatial and areal distribution of lunar mare deposits in mare Orientale and South Pole/Aitken basin: Implications for crustal thickness relationships. *Proc. Lunar Planet. Sci. Conf. 26th,* 1539–1540.

Zuber, M. T., D. E. Smith, S. C. Solomon, D. O. Muhleman, J. W. Head, J. B. Garvin, J. B. Abshire, and J. L. Bufton 1992. The Mars Observer Laser Altimeter investigation. *J. Geophys. Res.* **97,** 7781–7797.

Zuber, M. T., D. E. Smith, F. G. Lemoine, and G. A. Neumann 1994. The shape and internal structure of the Moon from the Clementine Mission. *Science* **266,** 1839–1843.